TIME-DEPENDENT BEHAVIOR OF CONCRETE MADE WITH HAWAIIAN AGGREGATES

Harold S. Hamada, Samuel Zundelevich, and Arthur N. L. Chiu,
University of Hawaii

The results from experimental studies on creep and shrinkage behavior of axially loaded cylinders and the camber and deflection behavior of simply supported rectangular prestressed concrete beams are reported. The nominal compressive strength of the Hawaiian aggregate concrete is 5,000 psi. The specimens were stored at 73 F and 50 percent relative humidity. Two lightweight and one normal-weight concrete mixes were used to manufacture the specimens. The cylinders were loaded to 0.25 f'_c, 0.40 f'_c, and 0.60 f'_c. The beams were loaded at third points with 750-lb loads. The span length of the beam was 15 ft. All Hawaiian aggregate concretes show larger ultimate shrinkage strain when compared with data in published literature. Hawaiian lightweight concretes have smaller ultimate shrinkage strain than does the Hawaiian normal-weight concrete.

•LIGHTWEIGHT and normal-weight concrete is widely used in construction in the state of Hawaii. Because of its wide usage, there is a need for a better understanding of the initial and time-dependent behavior of concrete members.

This paper discusses the results obtained from experimental studies on the creep and shrinkage behavior of axially loaded cylinders and the camber and deflection behavior of simply supported rectangular prestressed concrete beams. All specimens were made from concrete using Hawaiian aggregates.

Much research work has been done on the long-term behavior of manufactured lightweight and normal-weight concrete, and many theories have been advanced to describe the empirical information. However, no universally accepted theory exists. The published experimental information indicates that many variables affect the long-term behavior of concrete that is stressed.

Testing is the only satisfactory means of assessing the long-term creep and shrinkage behavior of concrete that is made from local aggregates. For this study, standard concrete cylinders were used; they either were free of stress for investigating shrinkage behavior or were subjected to constant axial stress for investigating creep behavior.

Accurate prediction of camber in prestressed concrete beams and girders becomes especially important in bridge construction to ensure required cast-in-place slab thickness and conformance with grade profiles. Initial and time-dependent deflections are important in building construction because excessively large deflections result in unsightly cracks.

For this study, simply supported rectangular concrete beams, manufactured with local aggregates, were used for investigating camber and deflection behavior. Calculated values using available procedures are compared with assessed loss of prestress, axial shortening, camber, and deflection.

The following notation is used in this paper.

CF_{LA} = correction factor for delayed time of loading;
C_L = creep coefficient defined as the ratio of creep strain to initial strain at the time of applying additional dead load;
C_t = creep coefficient at time t;

Sponsored by Committee on Concrete Superstructures.

$\overline{C}_t$ = average value of creep coefficient at time t;
C_{t_1} = creep coefficient for the noncomposite beam due to subsequently applied loads;
C_u = ultimate creep coefficient;
D = parameter in creep equation;
Fo = prestressing force at transfer (after elastic loss);
ΔF_t = total loss of prestress at time minus the initial elastic loss;
n = number of gauges;
t = time;
t_{LA} = age of concrete when loaded, days;
$\Delta(t)$ = deflection at any time t;
$(\Delta_i)_{Fo}$ = initial camber due to the initial prestress force, Fo;
$(\Delta_i)_{DL}$ = initial deflection caused by the beam's own weight;
$(\Delta_i)_L$ = initial deflection caused by additional loading;
ϵ_o = creep strain of i th gauge;
ϵ_o^1 = initial strain of i th gauge;
$\overline{\epsilon}_o^1$ = average value of initial strain, and
ϵ_u = ultimate creep strain.

UNIAXIALLY LOADED CONCRETE CYLINDERS

Laboratory Procedures

Standard 6-in. diameter concrete cylinders were loaded in uniaxial compression in accordance with ASTM C 512-69 recommendations. The constant axial load was maintained by placing steel coil springs in series with the concrete specimens.

The concrete specimens were moist-cured for the first 7 days after manufacture and housed in a controlled-environment room thereafter. The room temperature was maintained at 73.4 ± 2 F, and the relative humidity was maintained at 50 ± 4 percent. All specimens were loaded 28 days after manufacture.

Concrete Mixes

The nominal compressive strength selected was 5,000 psi. Three coarse aggregates were selected: (a) basalt rock from Kapaa Quarry, Oahu; (b) lightweight volcanite cinder, commercially called cinderlite, from Molokai; and (c) lightweight trachyte pumice, commercially called volcanite, from Hawaii. Concrete made from the basalt rock weighed approximately 152 lb/ft^3, whereas concretes made from the other two aggregates were lighter (124 lb/ft^3 for cinderlite and 121 lb/ft^3 for volcanite) and hereafter will be referred to as lightweight concrete.

The design mixes for the 5,000-psi concrete are given in Table 1. These mixes were obtained from a commercial vendor, and the mixes are used in construction projects. The actual 28-day compressive strengths for the mixes are as follows: basalt, 5,883 psi; cinderlite, 5,513 psi; and volcanite, 4,445 psi. Average values were obtained from testing a minimum of three cylinders for each mix. Many cylinders were tested prior to the 28th day to determine the effect of age on compressive strength.

Mathematical Expressions for Creep

For this paper, the mathematical expression selected to represent creep strain as a function of time is taken from Meyers et al. (1):

$$C_t = (t^{0.6})/(t^{0.6} + D)\, C_u \qquad (1)$$

The values for C_u and D are to be determined from tests.

Other mathematical functions have been proposed: for example, the hyperbolic formula by Ross (2) and Lorman (3); the power function by Shank (4); and the logarithmic function by Thomas (5), Hansen (6), and McHenry (7). Other forms have also been proposed, but they will not be discussed here. Kajfasz and Szulc (8) have published a study on the various expressions.

Test Results

The constant-stress tests were designed to sustain three stress levels: 0.25 f'_c, 0.40 f'_c, and 0.60 f'_c. It was speculated that the first two stress levels were within the linear portion of the stress-strain curve, and the third stress level would fall in the nonlinear range.

Figures 1, 2, and 3 show the creep plus shrinkage strain histories for the three concrete mixes. Initial strains due to elastic shortening at the time of loading are also shown. The horizontal axis shows time after the application of loads on the specimens. Each point in the figures represents an average of nine readings taken from three cylinders. Three gauge lines, spaced 120 deg along the circular perimeter, were selected on each cylinder. Change in cylinder length was measured with an 8-in. Whittemore gauge.

Figure 1 shows the data for the normal-weight concrete. The actual stress levels were different from the desired values, but all three stress levels fell in the linear range of the stress-strain curve. The curves passing through the data points are drawn arbitrarily to delineate each stress level.

Figure 2 shows the data for the concrete made from volcanite aggregates with the stress levels at 0.29 f'_c, 0.45 f'_c, and 0.67 f'_c. Although the first two stress levels were in the linear range, the third stress level was definitely in the nonlinear range of the stress-strain curve. For the first two stress levels, the creep plus shrinkage strains were not significantly different from those shown in Figure 1. However, the initial strains were much larger than those for the basalt mix, indicating a lower elastic modulus for the volcanite mix.

Figure 3 shows the data for the concrete made from cinderlite aggregates with stress levels at 0.23 f'_c, 0.36 F'_c, and 0.55 f'_c. By using the ratio of applied stress to initial strains, we can observe the following:

$$(0.23\ f'_c/450) \cong (0.36\ f'_c/839) \cong (0.55\ f'_c/1,171) \cong \text{elastic modulus}$$

Because these three ratios for the initial strains are nearly equal, the three curves shown in Figure 3 are for the linear range of the stress-strain curve.

Comparison of Figures 1 and 3 may show that the creep plus shrinkage strain of the lightweight cinderlite is less than that of the normal-weight concrete. However, the initial strains of the lightweight concrete are greater, and therefore the total strain (creep plus shrinkage plus initial strains) is greater for the lightweight concrete.

Figures 4, 5, and 6 show the time variation of the creep strain. These curves are similar to those shown in Figures 1, 2, and 3, except that shrinkage strains have been subtracted. The variation of shrinkage strain with time may be obtained from these figures by taking the difference between the appropriate curves. Special shrinkage strain versus time curves will not be presented. Shrinkage strains are discussed in more detail in subsequent portions of this paper.

The curves shown in Figures 4, 5, and 6 are based on the equation

$$\bar{\epsilon}_c = \epsilon_u(t^{0.6})/(t^{0.6} + D) \qquad (2)$$

The constants C_u and D, which are shown in Figures 4, 5, and 6, have been determined by least square fitting of the experimental data. It is noted that the creep coefficient for the normal-weight concrete is greater than that of the lightweight concrete. The creep coefficient for lightweight concrete from Hawaiian aggregates compares favorably with those given by Shideler (9).

In the process of determining C_u and $\bar{\epsilon}_u$ from the experimental data, the following problem was observed. The coefficients C_u and D were obtained by least square fitting of the average values of the creep coefficient.

Table 1. Design mixes for 5,000-psi concrete.

Mix	Material	Size	Source	ASTM Designation	Quantity
Mix 47[a]					
Coarse aggregate	Basalt	3/4 in.	Kapaa	C-33	1,575 lb
Fine aggregate	Basalt	Number 4	Kapaa	C-33	1,008 lb
	Sand	—	Molokai	C-33	546 lb
Cement	Type I	—	Hawn/Perm	C-150	7.2 sacks
Admixture	Plastiment	—	Sika	C-494	3 oz/sack
Mix 67[b]					
Coarse aggregate	Cinder	3/4 in.	Molokai	C-330	1,000 lb
Fine aggregate	Coral	Number 4	Barbers Point	C-33	619 lb
	Sand	—	Molokai	C-33	705 lb
Cement	Type I	—	Hawn/Perm	C-150	7.3 sacks
Admixture	Plastiment	—	Sika	C-494	3 oz/sack
Mix 77V[c]					
Coarse aggregate	Volcanite	3/4 in.	Hawaii	C-330	1,200 lb
Fine aggregate	Volcanite	Number 4	Hawaii	C-330	1,010 lb
Cement	Type I	—	Hawn/Perm	C-150	8.0 sacks
Admixture	Plastiment	—	Sika	C-494	3 oz/sack

[a]Mix 47 = 5,000-psi 3F with plastiment (5.0-3FP1-7.2).
[b]Mix 67 = 5,000-psi cinderlite with plastiment (5.0-CCP1-7.5).
[c]Mix 77V = 5,000-psi volcanite with plastiment (5.0-VOP1-8.0).

Figure 1. Creep plus shrinkage strains versus time after loading for basalt concrete.

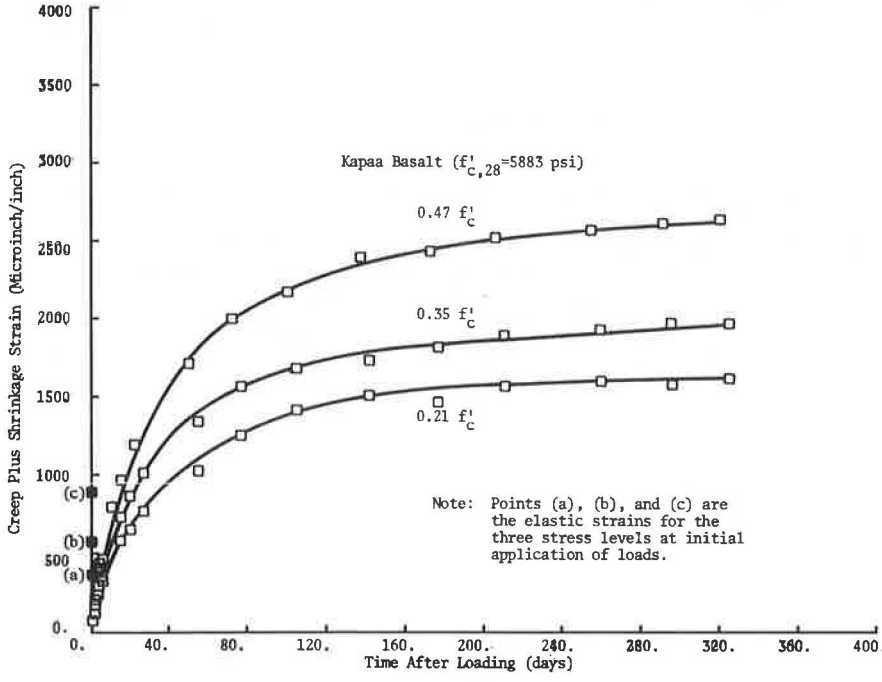

Figure 2. Creep plus shrinkage strains versus time after loading for volcanite concrete.

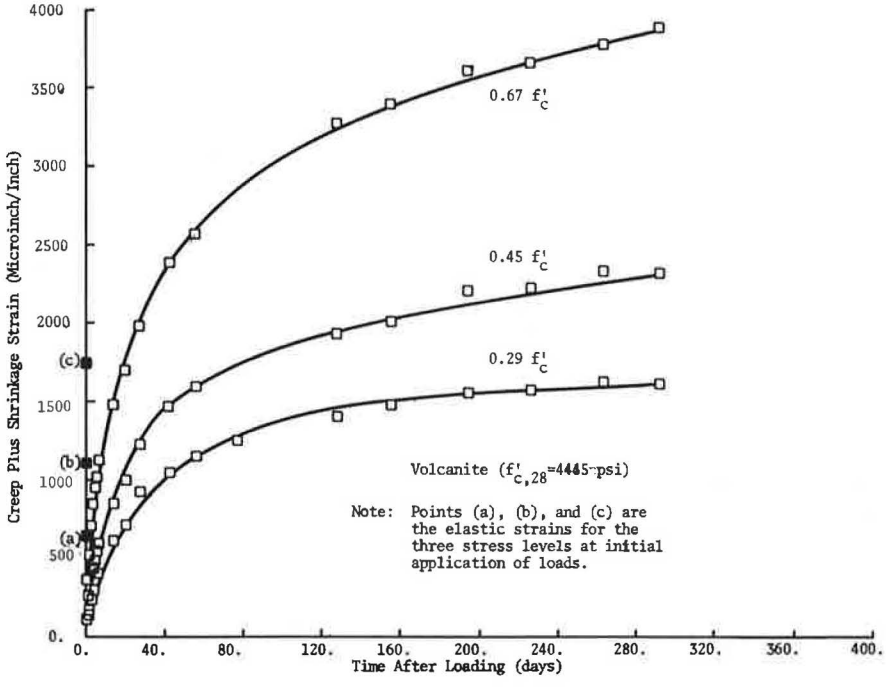

Figure 3. Creep plus shrinkage strains versus time after loading for cinderlite concrete.

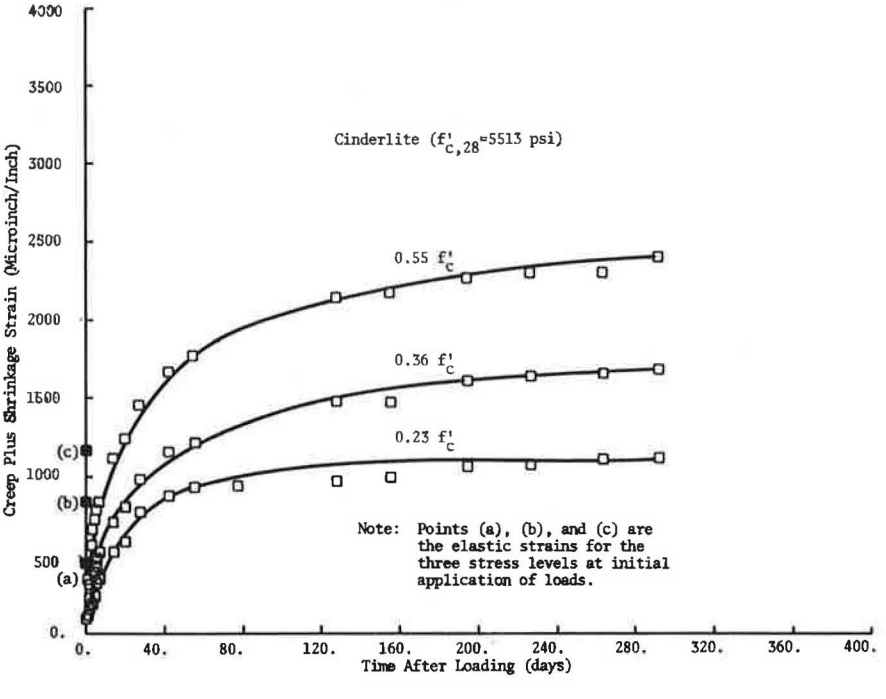

Figure 4. Creep strain versus time after loading for basalt concrete.

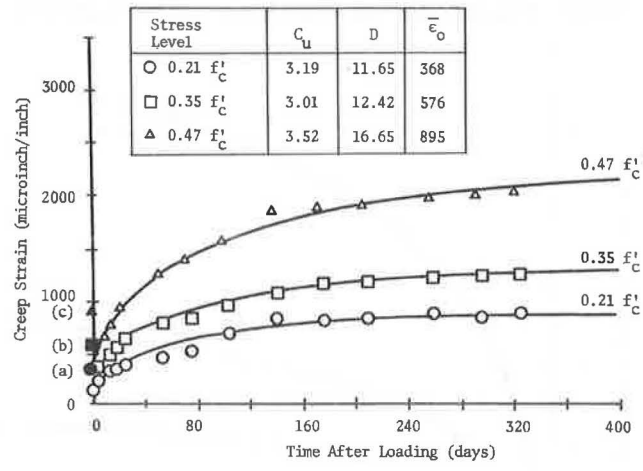

Figure 5. Creep strain versus time after loading for volcanite concrete.

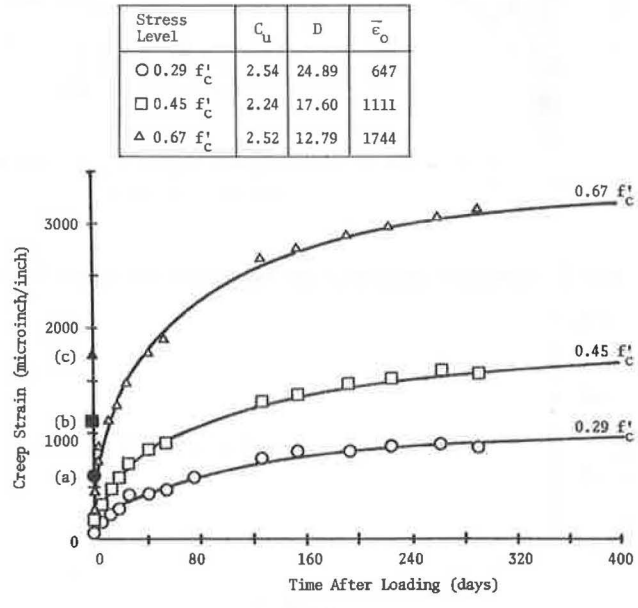

Figure 6. Creep strain versus time after loading for cinderlite concrete.

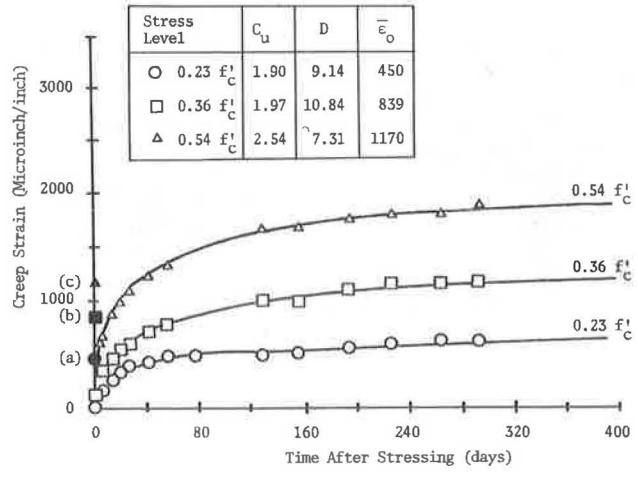

$$\overline{C}_t = \left[\sum_{i=1}^{n} (\epsilon_{o_1}/\epsilon_{o_1})\right]\Big/ n \qquad (3)$$

The average initial strain was determined by the equation

$$\overline{\epsilon}_o = \left[\sum_{i=1}^{n} (\epsilon_{o_1})\right]\Big/ n \qquad (4)$$

Now if one uses the product of $\overline{\epsilon}_o$ and C_u as the value of the ultimate creep strain ϵ_u in Eq. 2, the resultant curves will not adequately represent the data points. The ultimate creep strain ϵ_u must be determined separately. This observation may suggest that the creep coefficient is not a good parameter to use because it does not adequately demonstrate the variation in the experimental data in both numerator ϵ_{o_1} and denominator ϵ_{o_1}.

SIMPLY SUPPORTED PRESTRESSED CONCRETE BEAMS

Simply supported rectangular prestressed concrete beams were used to investigate the camber and deflection characteristics. These beams were manufactured with the same types of aggregates as were used for the cylinders. Type I standard cement and plastiment as a retardant admixture were used.

By using the different mixes, with a nominal strength F_c = 5,000 psi, three sets of specimens were cast separately. Each set consisted of three beams to study deflections and three beams to study camber (one unstressed beam 7 ft 9 in. long was poured for each set to determine shrinkage strains). The beams were 4 in. by 6 in. in cross section, 15 ft 6 in. long, and simply supported over a 15-ft span. Two $\frac{3}{8}$ in., 7-wire, 270^k strands located at 1.75 in. from the bottom were used for the prestressing. In addition to their own weights, the deflection specimens support two concentrated 750-lb loads at one-third points of the span as shown in Figure 7.

Strain readings were taken with a Whittemore gauge at different times in accordance with ASTM C 512-69. The gauge point locations are also shown in Figure 7. Camber and deflection values from dial gauge readings compared very well with values calculated by using strain-gauge point readings.

EXPRESSIONS USED TO CALCULATE CAMBER AND DEFLECTION

Several mathematical expressions are available to model the deflection behavior of prestressed concrete members. Reference 10 contains a simplified version from the more accurate expression developed by Branson (11). The terms in Branson's expression can be rearranged, and the total deflection, excluding the effects of non-prestressed reinforcement, can be expressed as the sum of different components shown in Eq. 5 and Figures 8 and 9.

$$\Delta(t) = \Delta_1 + \Delta_2(t) + \Delta_3 + \Delta_4(t) \qquad (5)$$

where

$$\Delta_1 = (\Delta_1)_{F_o} - (\Delta_1)_{D_L} \qquad (6)$$

is the result of the initial camber (positive) due to initial prestressing force and the initial deflection due to the beams's own weight;

$$\Delta_2(t) = \{-(\Delta F_t/Fo) + [1 - (\Delta F_t/2Fo)]C_t\}(\Delta_1)_{F_o} - C_t(\Delta_1)_{D_L} \qquad (7)$$

Figure 7. Prestressed concrete beams.

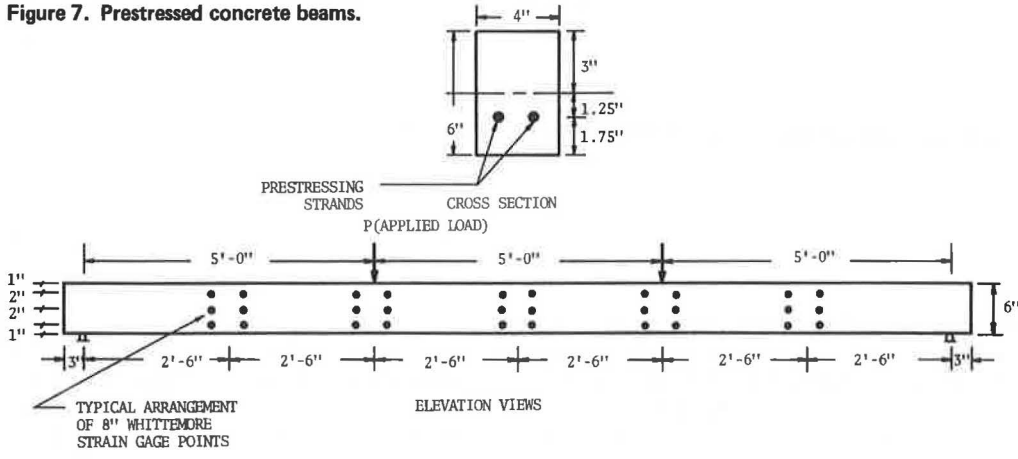

Figure 8. Camber and deflection behavior of simply supported prestressed concrete beams.

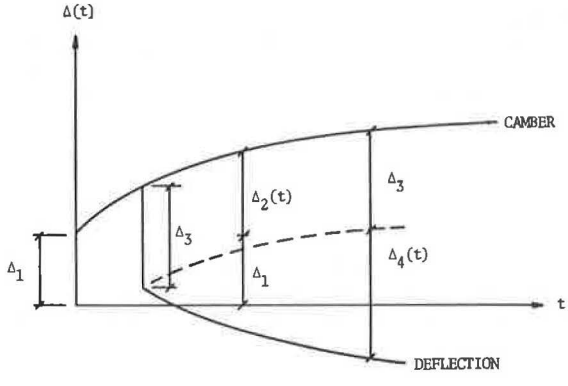

Figure 9. Components of deflection of a simply supported prestressed concrete beam.

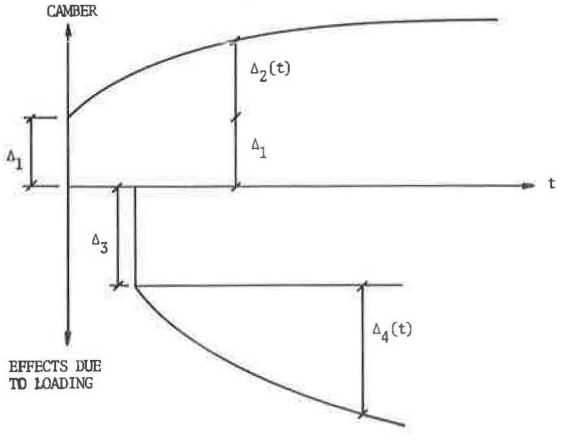

is the result of time-dependent effects due to initial camber;

$$\Delta_3 = -(\Delta_1)_{load} \tag{8}$$

is the change in deflection due to additional loading; and

$$\Delta_4(t) = -C_{t_1}(\Delta_1)_{load} - [-(\Delta F_1/2Fo)\, C_L - (\Delta F_t/2Fo)\, C_t\,]\,(\Delta_1)_{Fo} \tag{9}$$

is the time-dependent effect due to loading and includes the gain in prestress due to the lengthening of fiber at the level of the prestressing steel.

The equations adequately model the deflection behavior of a prestressed concrete member if proper values for concrete strength, modulus of elasticity, ultimate shrinkage strain, and ultimate creep coefficient are used. Conditions other than standard have to be considered by using correction factors to account for differences. Of particular importance are the values of the creep coefficient at any time and the correction factor due to age of loading represented by Eqs. 10 and 11. These equations were presented in detail elsewhere (1).

$$C_t = [t^{0.6}/(D + t^{0.6})]\, C_u \tag{10}$$

$$CF_{LA} = 1.25\, t_{LA}^{-0.118} \tag{11}$$

The parameters, C_u and D, are given in Figures 4, 5, and 6.

RESULTS

This section discusses the experimental results obtained from the study: compressive strength, modulus of elasticity, shrinkage, creep, loss of prestress, camber, and deflection.

Compressive Strength

Results from compression tests indicate that the cinderlite and volcanite mixes have higher early strengths than do the basalt mix.

The calculated modulus of elasticity, using the ACI formula, was always higher than the measured value. This could be one of the reasons why measured initial deflection values were higher than calculated values.

Shrinkage

Table 2 compares ultimate shrinkage strains and free shrinkage values derived from measurements on the free-standing beams. The measured shrinkage values are higher than those suggested by Meyers et al. (1); the latter could be used if no other information is available. However, variations in ultimate shrinkage values cause only minor changes in the answers when predicting camber and deflections. The time-dependent components of deflection, as calculated from Branson's method (using measured constants and measured shrinkage strains), were compared with calculated values by using suggested shrinkage strains. It was found that the behavior can be predicted with acceptable accuracy in both cases.

Creep

In contrast to the cylinder specimens, where the stresses are uniform and maintained constant, the beam specimens show stresses varying along the depth of the member and decreasing with time. To assess the experimental coefficients under such conditions, we obtained ultimate creep coefficients from the measured data. The procedure was to

fit the curves of the average measured camber [$\Delta_1 + \Delta_2(t)$] and the average measured effects on deflection due to a subsequently applied load [$\Delta_3 + \Delta_4(t)$]. However, to minimize the effects of the discrepancy in the initial camber and in the change in deflection , we normalized the camber and the effects on deflection due to applied loads by dividing the initial camber Δ_1 and instantaneous change in deflection due to loading Δ_3 respectively. If different coefficient values were used with the available expressions for the loss of prestress, camber, and deflection, the value yielding the best visual fit between experimental and calculated curves is selected as the most suitable. Branson's method and measured values of concrete strength and ultimate shrinkage strains were used in the calculations.

The normalized average measured camber and the normalized effects on deflection due to applied loads are shown in Figures 10, 11, and 12 for basalt, cinderlite, and valcanite. Also shown in the figures are curves using experimental constants and ultimate creep coefficients ($C_{u_{basalt}} = 3.7$, $C_{u_{cinderlite}} = 3.3$, and $C_{u_{volcanite}} = 3.0$) obtained by applying the method described in the previous paragraph. Notice that the theoretical curves for the basalt and volcanite mixes fit the experimental curves at every point; this proves the adequacy of Eq. 11. The small discrepancies observed for the cinderlite mix indicate that the values of the parameters in Eq. 11 for the cinderlite mix may be different from those shown (13). Eq. 10 yields excellent results for the three mixes.

Experimental values obtained from the beams as well as from the cylinders are compared with suggested ultimate creep coefficients in Table 2. Differences in values may be attributed to the sensitivity of the creep coefficient to variation of stresses along the depth of the section, to decreasing magnitude of the stresses due to the loss of prestress, and to the delayed time of loading. (The volume-surface ratio for the beams was approximately equal to the volume-surface ratio for the cylinders.)

Loss of Prestress

The initial time-dependent strains for each beam at all five sets of gauge points were measured at different times after stressing. A typical strain diagram at a midspan section is shown in Figure 13.

The loss of prestress was evaluated by using the strain at the level of the steel and by adding to it 75 percent of the calculated relaxation as suggested by Branson (11). The value of 75 percent takes into account the fact that stress relaxation occurs under decreased strain caused by creep and shrinkage. Experimental loss of prestress at midspan for each concrete mix is shown in Figure 14.

Measured values were compared with calculated values by using the methods suggested in Ref. 10 and by using Branson's method (11) along with suggested and measured constants. It was concluded that Branson's method with suitable constants will predict the loss of prestress more accurately. The method suggested in Ref. 10 is simplified to avoid extensive calculations in design.

Camber and Deflection

Camber and deflection histories for each beam measured with dial gauges are shown in Figures 15, 16, and 17. The average measured camber and average measured effects on deflection are separated and shown in Figures 18, 19, and 20.

Figures 18, 19, and 20 also show the camber and effects on deflection due to applied loads by using the respective recommended constants and formulas suggested elsewhere (10, 11). Also shown in the figures are curves obtained by Branson's method but which use creep coefficients experimentally determined from the beams and the cylinders. By using the experimental values from the beams, camber and deflection behavior can be predicted with better accuracy. The method suggested in Ref. 10 predicts the camber with acceptable accuracy but is less accurate in predicting the effects on deflection due to applied loads. This is because of simplifications made on ultimate creep coefficients for delayed time of loading. The essential difference between the method in Ref. 10 and Branson's method is that the former has been simplified to aid the designer.

Table 2. Comparison of experimental and suggested values for ultimate shrinkage strains and ultimate creep coefficients.

Type of Aggregate	Ultimate Shrinkage Strain, $\times 10^{-6}$ in./in.		Ultimate Creep Coefficient		
	Experimental	Suggested[a]	Experimental (from beams)	Experimental (from cylinders)	Suggested[a]
Basalt	1,050	714	3.7	3.24	2.69
Cinderlite	938	714	3.3	2.17	2.34
Volcanite	878	726	3.0	2.44	2.33

[a]Derived from Ref. 1.

Figure 10. Comparison of normalized camber and normalized effects of subsequently applied loads with suggested values (basalt).

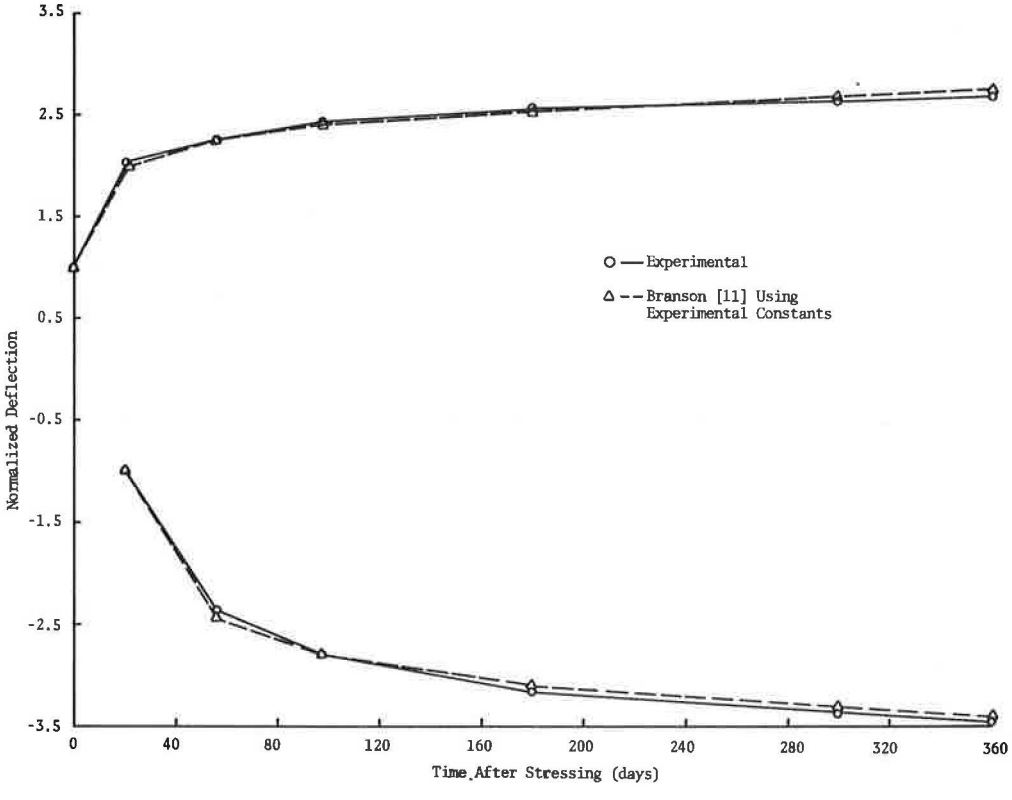

Figure 11. Comparison of normalized camber and normalized effects of subsequently applied loads with suggested values (cinderlite).

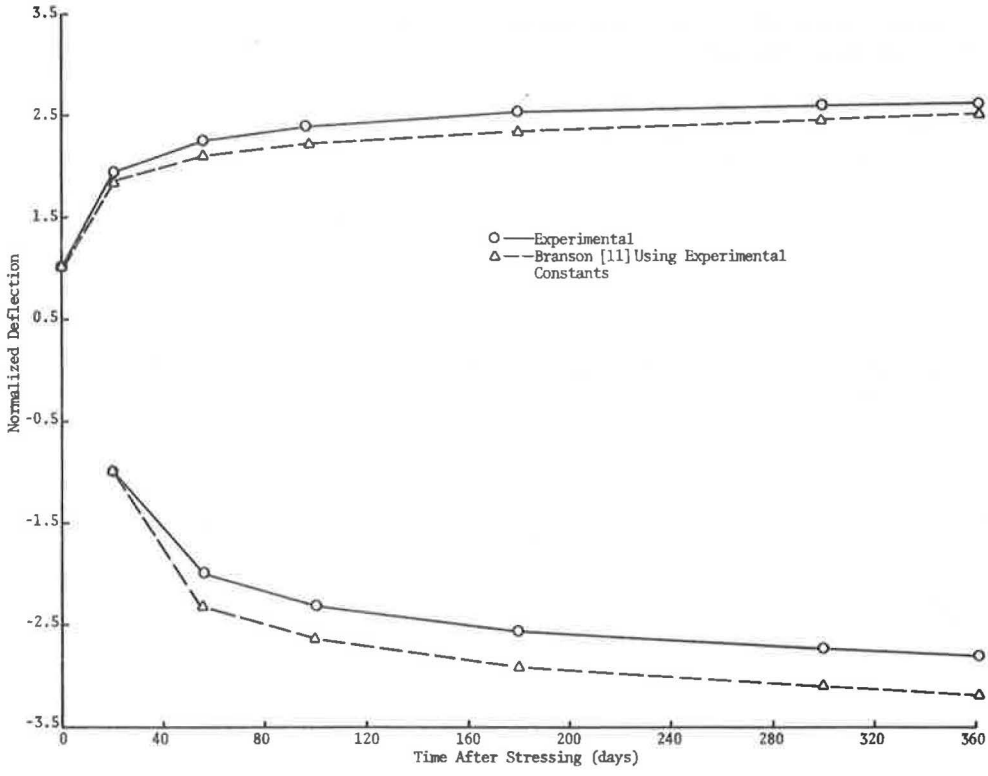

Figure 12. Comparison of normalized camber and normalized effects of subsequently applied loads with suggested values (volcanite).

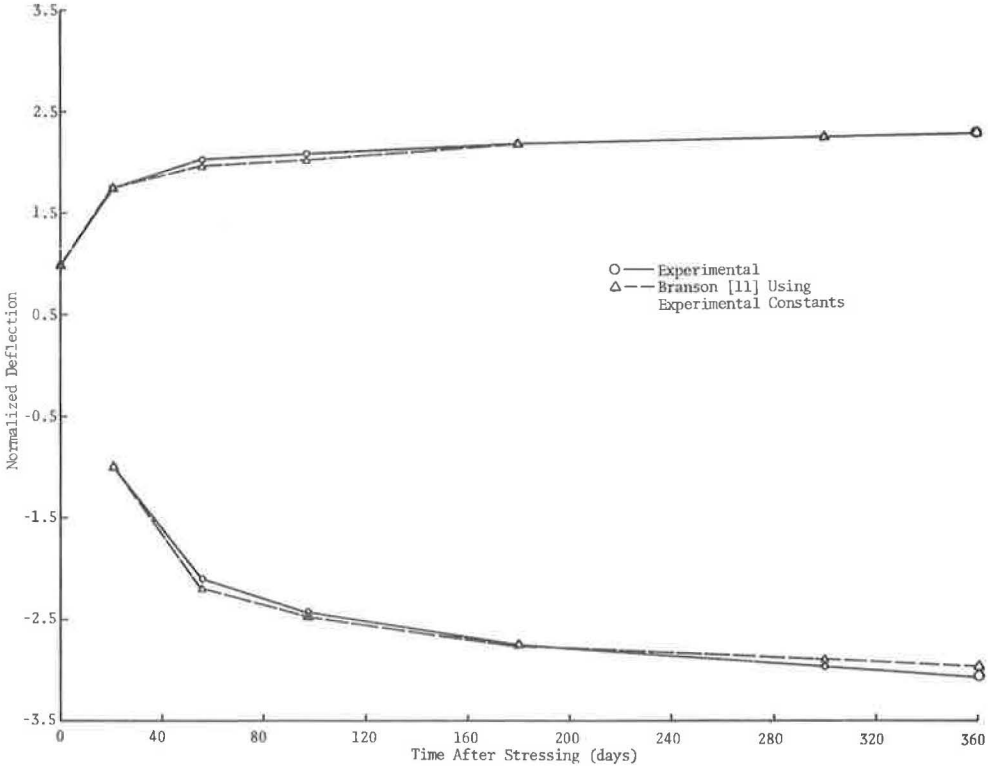

Figure 13. Typical measured strain diagrams at midspan for different times after stressing.

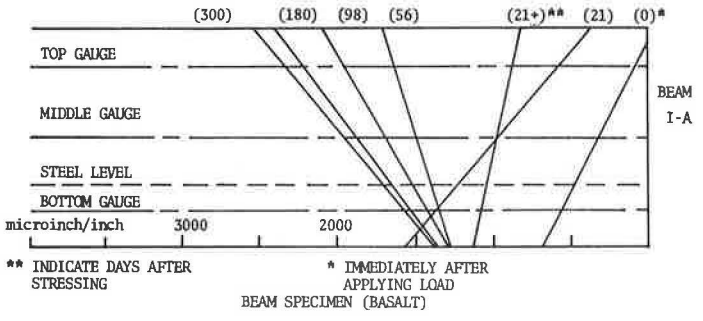

Figure 14. Experimental loss of prestress at midspan for each concrete mix.

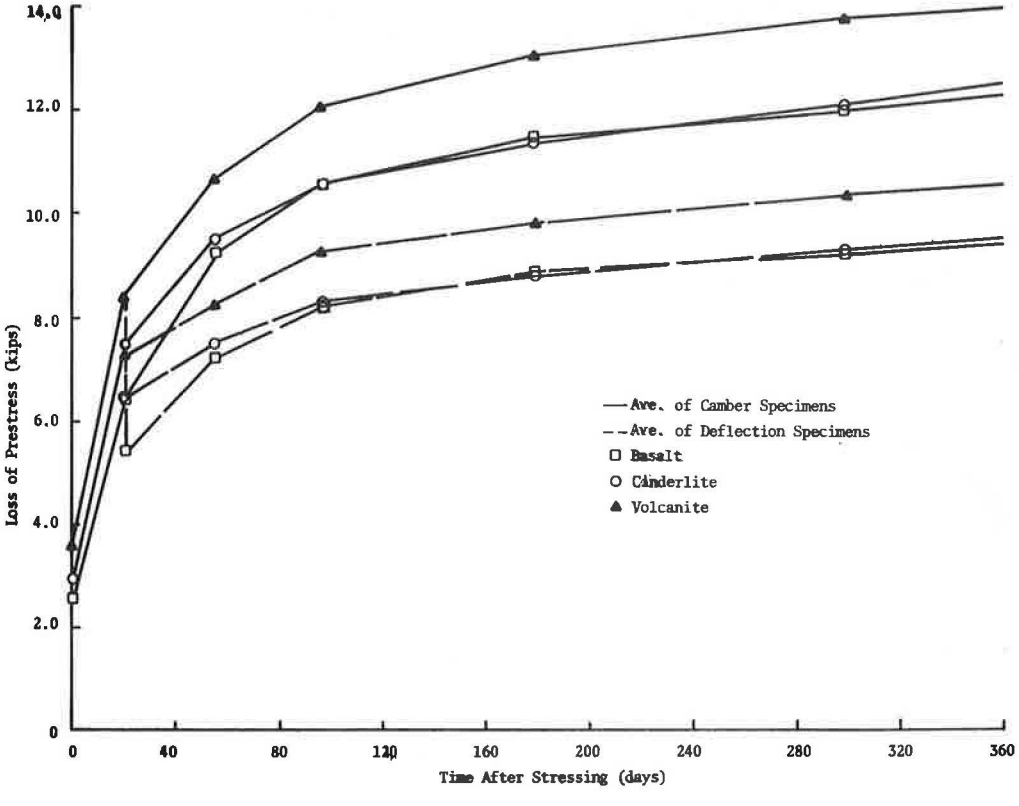

Figure 15. Measured deflection at midspan (basalt).

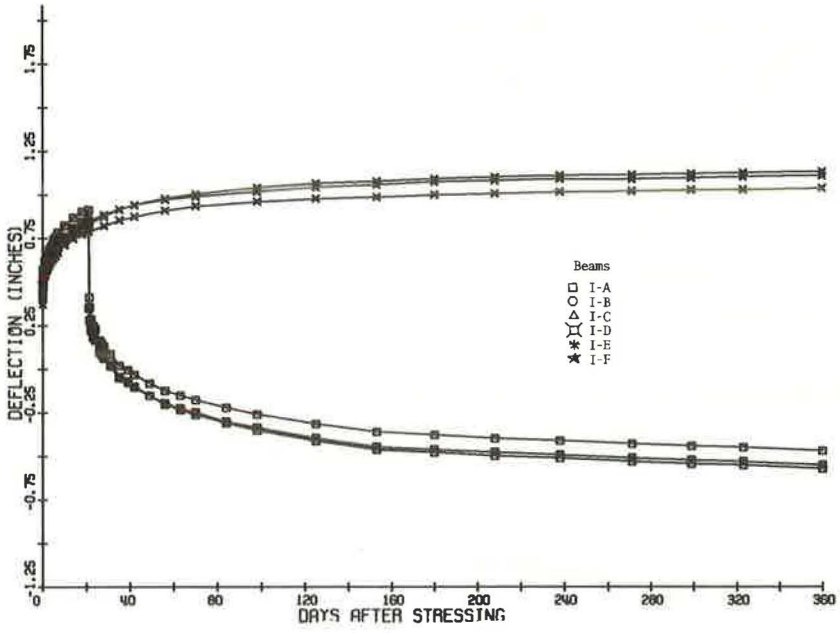

Figure 16. Measured deflection at midspan (cinderlite).

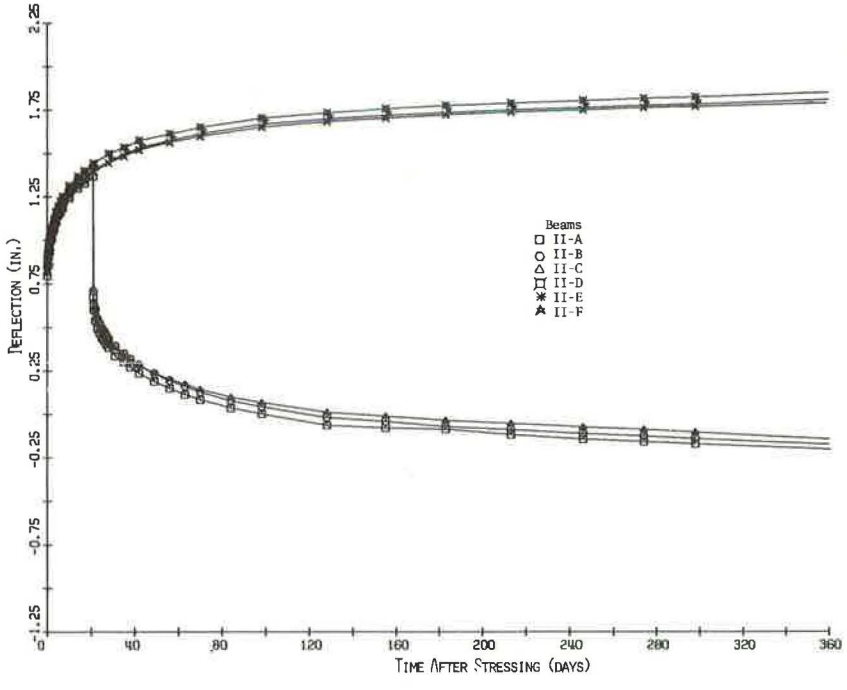

Figure 17. Measured deflection at midspan (volcanite).

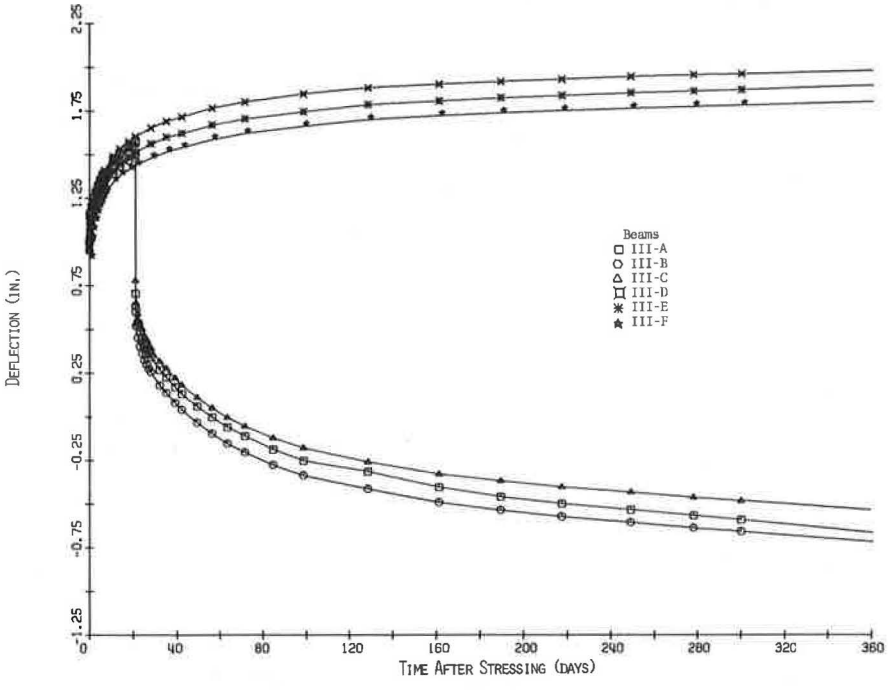

Figure 18. Comparison of camber and effects on deflection due to subsequently applied loads with suggested values using experimental strength (basalt).

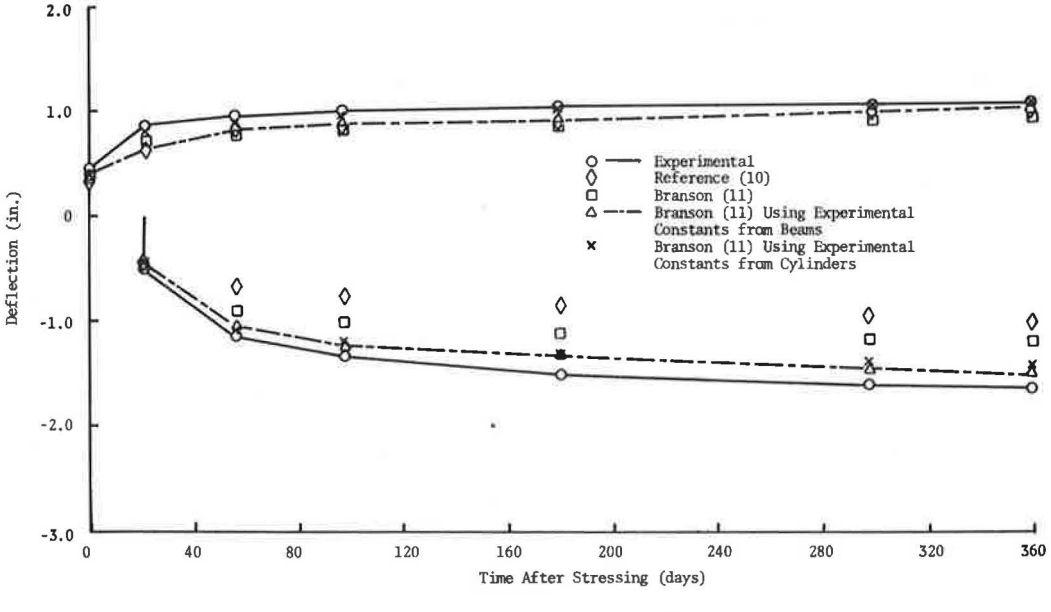

Figure 19. Comparison of camber and effects on deflection due to subsequently applied loads with suggested values using experimental strength (cinderlite).

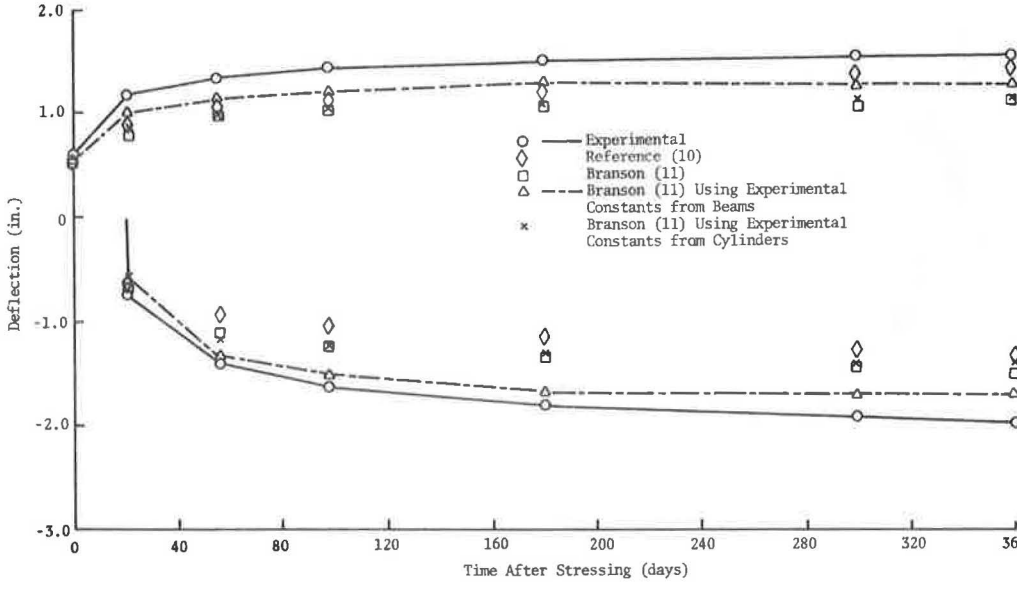

Figure 20. Comparison of camber and effects on deflection due to subsequently applied loads with suggested values using experimental strength (volcanite).

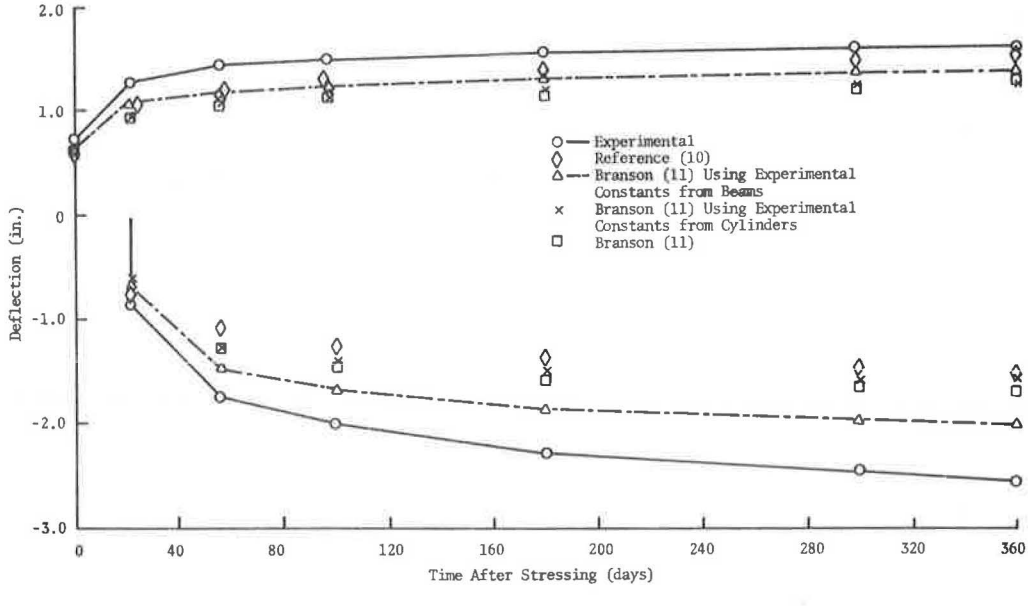

CONCLUSIONS

The following statements can be made on the basis of the study results.

1. Volcanite concrete has higher early strength relative to cinderlite and basalt concretes.
2. The moduli of elasticity for Hawaiian aggregate concretes are lower than the elastic modulus calculated from the ACI formula.
3. All Hawaiian aggregate concretes show larger ultimate shrinkage strains when compared with the data in published literature.
4. Hawaiian lightweight concretes have smaller ultimate shrinkage strain than the Hawaiian normal-weight concrete.
5. Differences in the ultimate creep coefficients, which were determined from uniaxially stressed concrete cylinders and prestressed concrete beams, may be attributed to large sensitivity to the loss of prestress, which is most difficult to assess.
6. The creep coefficient for basalt concrete is larger than the creep coefficients for cinderlite and volcanite concretes. However, this does not necessarily mean that the basalt concrete creeps more because the creep strain is determined from the product of the creep coefficient and initial strains.
7. Branson's method for predicting initial and time-dependent loss of prestress, axial shortening, camber, and time-dependent deflection are recommended. The data show that this method accurately estimates these effects if appropriate coefficients are used for concrete made from Hawaiian aggregates.

ACKNOWLEDGMENT

The work described in this paper was carried out in the Civil Engineering Department at the University of Hawaii. It forms part of a research program on the time-dependent behavior of concrete made from Hawaiian aggregates, which is financed by research grants from the Hawaii Department of Transportation.

REFERENCES

1. Meyers, B. L., Branson, D. E., Schumann, C. G., and Christianson, M. L. The Prediction of Creep and Shrinkage Properties of Concrete. Iowa State Highway Commission Res. Rept. 70-5, Aug. 1970.
2. Ross, A. D. Concrete Creep Data. The Structural Engineer, London, Aug. 1937, p. 314.
3. Lorman, W. R. The Theory of Concrete Creep. Proc. ASTM, Vol. 40, 1940, p. 1,082.
4. Shank, J. R. The Plastic Flow of Concrete. Ohio State Univ. Bull. 91, 1935.
5. Thomas, F. G. A Conception of the Creep of Unreinforced Concrete, and an Estimation of the Limiting Values. The Structural Engineer, London, Vol. 11, No. 2, Feb. 1933.
6. Hansen, T. C. Creep and Stress Relaxation of Concrete, A Theoretical and Experimental Investigation. Proc. Swedish Cement and Concrete Research Institute, Stockholm, 1960, p. 98.
7. McHenry, D. A New Aspect of Creep in Concrete and Its Application to Design. Proc. ASTM, Vol. 43, 1943, p. 1,069.
8. Kajfasz, S., and Szulc, J. Approximation of Experimental Data by a Creep Function. Materiaux et Constructions, Vol. 3, No. 18, 1970, p. 381.
9. Shideler, J. J. Lightweight Aggregate Concrete for Structural Use. Portland Cement Association Bull. D 17, Skokie, Illinois, 1957.
10. Branson, D. E. Design Procedures for Computing Deflections. ACI Jour., Proc., Vol. 65, No. 9, Sept. 1968, p. 730.
11. Branson, D. E., Meyers, B. L., and Kripanarayanan, K. M. Loss of Prestress, Camber and Deflection of Noncomposite and Composite Structures Using Different Weight Concretes. Iowa State Highway Commission Res. Rept. 70-6, Aug. 1970.

12. Hamada, H. S., Watari, J., and Chiu, A. N. L. Creep and Shrinkage of Concrete Made From Hawaiian Aggregates. Dept. of Civil Eng., Univ. of Hawaii, Tech. Rept. R 71-2 (to be published).
13. Zundelevich, S., Lee, D. N. L., and Chiu, A. N. L. Camber and Deflection Behavior of Simply Supported Prestressed Concrete Beams Manufactured With Hawaiian Aggregates. Dept. of Civil Eng., Univ. of Hawaii, Tech. Rept. R 71-1 (to be published).